Investigation of Mg(BH 4)(NH 2)-Based Composite Materials with Enhanced Mg 2+ Ionic Conductivity

Ronan Le Ruyet, Romain Berthelot, Elodie Salager, Pierre Florian, Benoit Fleutot, Raphaël Janot

Investigation of $Mg(BH_4)(NH_2)$-Based Composite Materials with Enhanced Mg^{2+} Ionic Conductivity

Ronan LE RUYET[a,d], Romain BERTHELOT[b,d], Elodie SALAGER[c,d], Pierre FLORIAN[c], Benoît FLEUTOT[a,d,*], Raphaël JANOT[a,d,*]

[a] *Laboratoire de Réactivité et Chimie des Solides (LRCS), Université de Picardie Jules Verne, UMR 7314 CNRS, 33 Rue Saint Leu, Amiens 80039, France.*
[b] *Institut Charles Gerhardt Montpellier (ICGM), Université de Montpellier, UMR 5253 CNRS, Montpellier 34095, France.*
[c] *Conditions extrêmes et Matériaux : Haute Température et Irradiation (CEMHTI), UPR 3079 CNRS, Université d'Orléans, 1D Avenue de la Recherche Scientifique, Orléans 45071, France.*
[d] *Réseau sur le Stockage Electrochimique de l'Energie (RS2E), FR 3459 CNRS, 33 Rue Saint Leu, Amiens 80039, France.*

* Corresponding authors: B. Fleutot: benoit.fleutot@u-picardie.fr
R. Janot: raphael.janot@u-picardie.fr

Abstract

Nowadays, the development of rechargeable Mg batteries remains a challenge, especially due to the difficulty to find a non-corrosive liquid electrolyte with suitable ionic transport properties. A possible improvement could come from a solid electrolyte, such as $Mg(BH_4)(NH_2)$, which has been recently reported as a solid-state Mg-ion conductor. In this study, its synthesis parameters are carefully investigated. The formation of an additional phase is reported, whose amount is decreased by optimizing the synthesis parameters and especially by increasing the ball-milling speed. For the first time, ^{11}B MAS-NMR spectroscopy is applied to this Mg-B-N-H system: it reveals that an additional phase is always present even in an amorphous state. Interestingly, it strongly influences the ionic conduction properties. Indeed, the as-obtained borohydride-amide composite exhibits a high conductivity of 3.10^{-6} $S.cm^{-1}$ at 100°C, one of the highest ever-reported ionic conductivity for a Mg^{2+} solid conductor at such low temperature.

1. INTRODUCTION

Rechargeable Mg batteries are nowadays developed to go beyond Li-ion batteries. Interest rose for this new technology because magnesium has promising characteristics as negative electrode: a low redox potential (-2.356 V vs. SHE, relatively close to the potential of -3.040 V achieved by metallic lithium), a higher volumetric energy than lithium (3833 $mAh.cm^{-3}$ vs. 2062 $mAh.cm^{-3}$) and a large abundance in the earth crust.[1] Nevertheless, since 2000 and the first Mg-ion rechargeable battery with a liquid electrolyte reported by Aurbach et al.,[2] the development of viable systems remains difficult. A very severe issue concerns the liquid electrolyte. Indeed, conventional carbonate-based liquid electrolytes cannot be used in Mg batteries because of the formation of a blocking layer at the surface of the magnesium electrode.[3] Consequently, new electrolytes have been specifically developed for Mg-ion batteries. The most common liquid electrolytes for Mg batteries are based on Grignard reagents, i.e. organo-aluminate complexes $Mg(AlCl_{4-n}R_n)_2$, which are solvated in organic solvents such as tetrahydrofuran (THF). Nevertheless, they are strongly corrosive due to Cl^- anions and suffer from a low electrochemical stability window (below 2 V vs. Mg^{2+}/Mg).[1,3,4] More recently, Mohtadi et al. have studied halogen-free liquid electrolytes using complex hydrides as $Mg(BH_4)_2$ in THF or monoglyme and $Mg(CB_{11}H_{12})_2$ in tetraglyme. This has led to significant improvements with an electrochemical stability up to 3.8 V vs. Mg^{2+}/Mg for the latter.[5,6]

The replacement of these liquid electrolytes by a solid state ionic conductor could be a solution. Previous studies have reported Mg^{2+} ion conducting materials as $MgS\text{-}P_2S_5\text{-}MgI_2$ glasses[7] and Mg-containing NASICON materials such as $MgZrPO_4$, $MgZr_4(P_6O_4)_6$ and other $Mg_xZr_y(PO_4)_z$ compositions.[8–10] Even so, these materials reach a significant ionic conductivity only at high temperatures: 10^{-7} $S.cm^{-1}$ at 200°C and 10^{-6} $S.cm^{-1}$ at 500°C for the sulfide-based glasses and for the NASICON phases, respectively. Recently, Roedern et al. have demonstrated a high ionic conductivity of $6x10^{-5}$ $S.cm^{-1}$ at 70°C in a solid compound obtained by the complexation of $Mg(BH_4)_2$ by ethylene-diamine molecules.[11] However, the electrochemical stability of this new phase is limited to 1.2 V vs. Mg^{2+}/Mg. Previously, Higashi et al. have reported a promising ionic conductivity of 10^{-6} $S.cm^{-1}$ at 150°C for the inorganic compound $Mg(BH_4)(NH_2)$, a conductivity which is three orders of magnitude

higher than the one of $Mg(BH_4)_2$.[12] This compound is similar to the already known Li^+ ion conductor $Li_2(BH_4)(NH_2)$, which exhibits a conductivity of $2x10^{-4}$ $S.cm^{-1}$ at room temperature.[13] $Mg(BH_4)(NH_2)$ was synthesized for the first time by Noritake et al. from a ball-milled mixture of $Mg(BH_4)_2$ and $Mg(NH_2)_2$.[14] X-ray diffraction synchrotron measurements were performed at different temperatures. They observed the crystallization of $Mg(BH_4)(NH_2)$ at around 150°C. Its crystal structure was solved in a tetragonal unit cell with the space group $I4_1$ and a density of 0.9966 $g.cm^{-3}$. This low density is very interesting for a solid-state electrolyte as it allows obtaining good ionic percolation in composite electrodes with a relatively low weight of electrolyte, ensuring reasonable electrochemical gravimetric capacities for the composite electrodes. Higashi et al. have also investigated the potential application of this phase as a solid electrolyte.[12] They calculated a band gap of 4.9 eV demonstrating that the material is an electronic insulator. The possible use as an electrolyte was confirmed by reversibly depositing and stripping magnesium in a $Mg/Mg(BH_4)(NH_2)/Pt$ electrochemical cell and they have estimated its electrochemical stability from 0 V to at least 3V vs. Mg^{2+}/Mg. These results are very promising but the few studies on $Mg(BH_4)(NH_2)$[12,14–16] did not detail the synthesis parameters and how the sample purity might influence the material properties, especially the ionic conductivity.

In this work, we have carefully investigated the synthesis parameters of $Mg(BH_4)(NH_2)$. The purity of the sample has been evaluated by X-ray diffraction coupled with ^{11}B MAS-NMR spectroscopy which has been performed for the first time on this compound. These analyses reveal the presence of an additional phase, in addition to crystalline $Mg(BH_4)(NH_2)$, having a strong impact on the ionic conductivity values.

2. EXPERIMENTAL

2.1. Synthesis

The different materials have been synthesized by solid-state synthesis with an equimolar amount of γ-$Mg(BH_4)_2$ (> 95 %, Sigma Aldrich) and $Mg(NH_2)_2$, the latter previously synthesized by ball-milling and annealing of MgH_2 (> 99 %, Sigma Aldrich) under NH_3 gas (99.9 %, Messer) following a synthesis method described in other studies.[17–19] The

two precursors were homogeneously mixed in an agate mortar within an argon filled glovebox. Then, 1 g of the mixture was transferred into a 50 cm^3 airtight tungsten carbide (WC) milling vial with 5 WC balls of 10 mm diameter corresponding to a powder to balls weight ratio of 1:38. The ball-milling was done with a Retsch PM100 at different milling speeds: from 100 rpm to 400 rpm for 1 h with a 2 min break every 30 min. Subsequently, the powder was pressed under 4 tons into a pellet of 13 mm diameter and annealed in a hermetic stainless-steel reactor sealed with a copper ring. The following annealing parameters were also studied: the time (from 48 h to 96 h), the temperature (from 120°C to 130°C) and the atmosphere (1 bar of Ar or 10 bar of H_2).

2.2. X-ray diffraction

Powder X-ray diffraction (PXRD) was performed on a Bruker D8 diffractometer using Co $K_{\alpha1}$-$K_{\alpha2}$ radiation in a θ-θ configuration. The acquisition of the diffraction patterns was done within a range of 2θ from 10 to 50° with steps of 0.023° and an exposure time of 2 s (cf. Figure 1a) and a longer acquisition was done on sample C from 16 to 50° with steps of 0.015° and an exposure time of 20 s (cf. Figure 1b). To avoid any contact of the samples with air, a hermetic sample holder with a Be window developed in the laboratory was used.[20]

2.3. NMR spectroscopy

^{11}B solid-state MAS-NMR spectroscopy measurements were performed using a 20 T Avance III Bruker spectrometer operating at 272.7 MHz using a 2.5 mm CP-MAS probe. All samples were handled and packed in rotors in an Ar filled glovebox. The spectra were obtained at a magic angle spinning rate of 30 kHz under pure nitrogen at 278 K. A one pulse ^{11}B experiment was recorded with a RF power of 50 kHz and a short excitation pulse (π</18). Spinal-64 ^{1}H heteronuclear decoupling was applied at 100 kHz during acquisition (8 ms). All spectra are referenced to a 1 $mol.L^{-1}$ solution of B_2O_3 set at 20.5 ppm and processed with a 3 Hz exponential broadening. Baseline correction and removal of the probe background were performed using a home-made Matlab program. The spectra were fitted with the DMfit software[21] under the assumption of two components with a first order quadrupolar interaction under finite MAS. The composition reported here are obtained from the fits of the whole spinning sideband pattern. The error in the fit was determined by a Monte Carlo procedure in

DMfit. For each sample, 500 spectra were generated by adding random noise with a Gaussian distribution to the experimental data and subsequently fitted. The resulting fitting parameters were statistically analyzed considering a normal distribution and the 95% confidence interval was extracted for each parameter. This interval is smaller than the experimental error for all the parameters.

2.4. Electrochemical Impedance Spectroscopy

Electrochemical Impedance Spectroscopy (EIS) measurements were realized with a MTZ-35 frequency response analyzer (BioLogic Company) coupled with an Intermediate Temperature System (ITS) controlling the sample temperature by Peltier effect. The different synthesized materials were cold pressed into pellets of 13 mm diameter under a pressure of 6 tons with around 100 mg of powder per pellet. A thickness of about 0.8 mm is obtained, corresponding to a density close to 95% of the theoretical one of $Mg(BH_4)(NH_2)$ (calculated from the crystallographic density: 0.9966 $g.cm^{-3}$). The pellets were sandwiched between two Papyex foils (flexible graphite previously dried under vacuum at 150°C) enhancing the electrical contacts between the pellet surface and the Controlled Environment Sample Holder (CESH) gold disks. The combined Papyex foil and gold disk ensure an ion blocking electrode. The electrolyte pellet is transferred under argon (in glovebox) into an asymmetric CESH to be sandwiched between the two ion blocking Papyex-gold electrodes. The CESH is then placed in ITS and AC impedance spectra were recorded in the frequency range from 30 MHz to 500 mHz with an excitation signal of 50 mV amplitude and from 50°C to 100°C upon heating and cooling ($1°C.min^{-1}$) with a temperature stabilization of 15 min before impedance measurement every 10°C.

2.5. Thermal stability

Differential Scanning Calorimetry (DSC) measurements were carried out on a Netzsch DSC 204 F1 heat flux differential calorimeter at a heating rate of $5°C.min^{-1}$ under a constant argon flow of 50 $mL.min^{-1}$. The samples were placed in aluminum crucibles which were sealed in a glovebox filled with argon and their lids were pierced under argon flow prior to the measurement to allow gas release upon heating. Gas mass spectrometry was done on a quadrupole QMS403D Aëolos® mass spectrometer with a stainless steel capillary heated at

230°C and a SEV detector (Channeltron). The counting time for mass spectrometer is of 20 ms per m/z values (scanning width: m/z = 1-100) with a resting time of 1 s. This measurement was performed under Ar atmosphere in a glovebox.

3. RESULTS AND DISCUSSION

3.1. Synthesis of $Mg(BH_4)(NH_2)$

The synthesis procedure of $Mg(BH_4)(NH_2)$ is described in previous papers[14-15] but the ball-milling and annealing parameters are not given. Thus, different parameters had to be tried to obtained crystalline $Mg(BH_4)(NH_2)$ with the highest possible purity (cf. Figure S1 and Table S1 in Supporting information). Starting with a low ball milling speed (200 rpm) and an annealing under Ar, the as-obtained material is not pure crystalline $Mg(BH_4)(NH_2)$. Then, a longer annealing improves the purity. Finally, it is only by increasing the ball-milling speed to 400 rpm and performing the annealing under 10 bar of H_2 that pure crystalline $Mg(BH_4)(NH_2)$ is observed by X-ray diffraction. In this paper, the focus is put on three samples (hereafter named A, B and C). These samples were chosen because they allow finding a relationship between the purity and the ionic conduction properties. Figure 1a shows the diffractograms obtained by PXRD of the samples A, B and C, the diagrams being smoothed and normalized in order to facilitate the comparison between them.

The synthesis parameters used for sample A are: a ball-milling at 200 rpm followed by an annealing at 130°C for 48 h under 1 bar of Ar. In this sample, two crystalline phases can be observed: $Mg(BH_4)(NH_2)$ (crystallizing in the space group $I4_1$) and an additional phase. This additional phase is similar to the one reported by Noritake et al. in their synchrotron X-ray diffraction measurements at different temperatures. In their study, this additional phase is seen between 70°C and 100°C meanwhile $Mg(BH_4)(NH_2)$ starts to crystallize and remains the only crystalline phase at 150°C.[14]

A longer annealing has been performed for sample B (96 h instead of 48 h) and at a lower temperature (120°C). The quantity of the crystalline additional phase decreases (cf. Figure 1a) but these parameters do not allow to obtain pure crystalline $Mg(BH_4)(NH_2)$. After the synthesis of these two samples, it has been considered that this additional phase could be

formed from the decomposition of one of the reactants because of the foamy aspect of the pellets, which suggests that some gas release occurs upon annealing. Another synthesis has been done with the annealing performed under 10 bar of H_2 to tackle this possible gas release issue. However, if this hydrogen pressure was successful to stop the gas release (no more foamy aspect), the product was nevertheless still impure and the reaction not completed as shown in Figure S1.

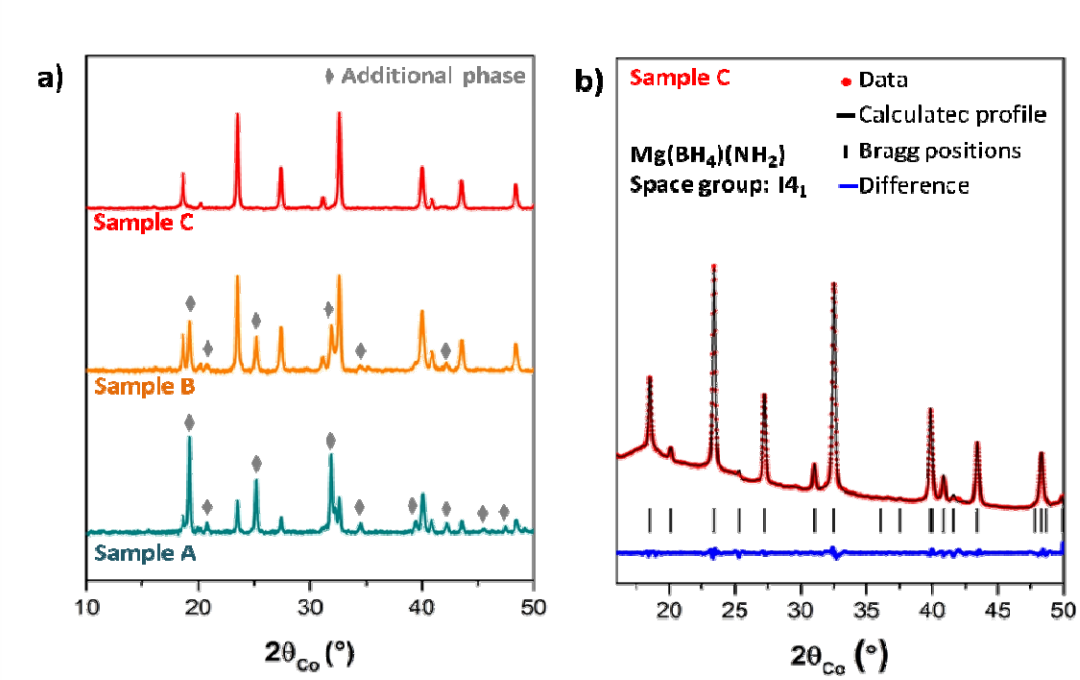

Figure 1. PXRD patterns (**a)** of samples A, B and C. (**b)** Profile matching of the diffraction pattern of sample C.

By increasing the ball milling speed, the purity of crystalline $Mg(BH_4)(NH_2)$ is greatly improved. Indeed, sample C was synthesized with a faster ball milling speed of 400 rpm and annealed at 120°C for 72 h under 10 bar of H_2. As presented in Figure 1a, the diffraction peaks from $Mg(BH_4)(NH_2)$ are well defined by XRD. Performing a profile matching for the sample C diffractogram (cf. Figure 1b), all reflections can be indexed in the tetragonal unit cell with space group $I4_1$. The refined unit cell parameters are a = 5.779(2) Å, c = 20.509(7) Å and V = 684.8(3) $Å^3$, close to the ones of the literature (a = 5.814(1) Å, c = 20.450(4) Å, V = 691.3(2) $Å^3$).[14]

From these observations, it results that the additional phase could have a different composition in magnesium borohydride and magnesium amide with a stoichiometry $Mg_{x+y}(BH_4)_{2x}(NH_2)_{2y}$, similar to what was reported for lithium-based compounds. In the case of $Li_2(BH_4)(NH_2)$ and $Li_4(BH_4)(NH_2)_3$, the formation of unstable substoichiometric phases with compositions $Li_{4-y}(BH_4)(NH_2)_{3-y}$ and $Li_{4-x}(BH_4)_{2-x}(NH_2)_2$ was observed.[22,23] Unfortunately, this additional phase $Mg_{x+y}(BH_4)_{2x}(NH_2)_{2y}$ cannot be obtained pure, making the XRD pattern analysis complex and the precise determination of its space group and unit cell parameters impossible at the moment.

3.2. ^{11}B MAS-NMR spectroscopy

To verify the purity of our materials and the local environment of boron in $Mg(BH_4)(NH_2)$, ^{11}B MAS-NMR analyses were performed for the first time on these materials. No peaks are detected around -20 ppm which indicate that no B_xH_y borane groups as $(B_3H_8)^-$, $(B_{12}H_{12})^{2-}$, $(B_{10}H_{10})^{2-}$ and BH_3 are present.[24–26] In Figure 2, the three ^{11}B NMR spectra display strong peaks between -37 ppm and -40 ppm, which can be unambiguously attributed to $(BH_4)^-$ anions.[27-28] Samples A and B show actually two peaks in this chemical shift area: a first one at about -37.6 ppm and a second one at about -39.6 ppm (cf. Figure 2b). We can consider that one of the NMR peak is due to $(BH_4)^-$ in $Mg(BH_4)(NH_2)$ and the other one to $(BH_4)^-$ in a slightly different environment as in the additional phase detected by XRD. To assign the two peaks, the spectra (including the spinning sideband patterns, cf. Figure S2) were fitted with two components and the percentage of boron atoms contributing to each environment (cf. Figure 2c) was extracted and compared to the relative proportion of the two crystalline phases observed by XRD analyses (cf. Figure 1). The percentage of boron atoms corresponding to the peak at -37.6 ppm increases from sample A to sample B, so with increasing proportion of $Mg(BH_4)(NH_2)$. In the same time, the percentage of boron atoms contributing to the peak at -39.6 ppm decreases from sample A to sample B, with the decrease of the additional phase content. We conclude therefore that the peak at -37.6 ppm is due to the $(BH_4)^-$ anions in $Mg(BH_4)(NH_2)$ and that the second peak at -39.6 ppm is due to $(BH_4)^-$ present in the additional phase.

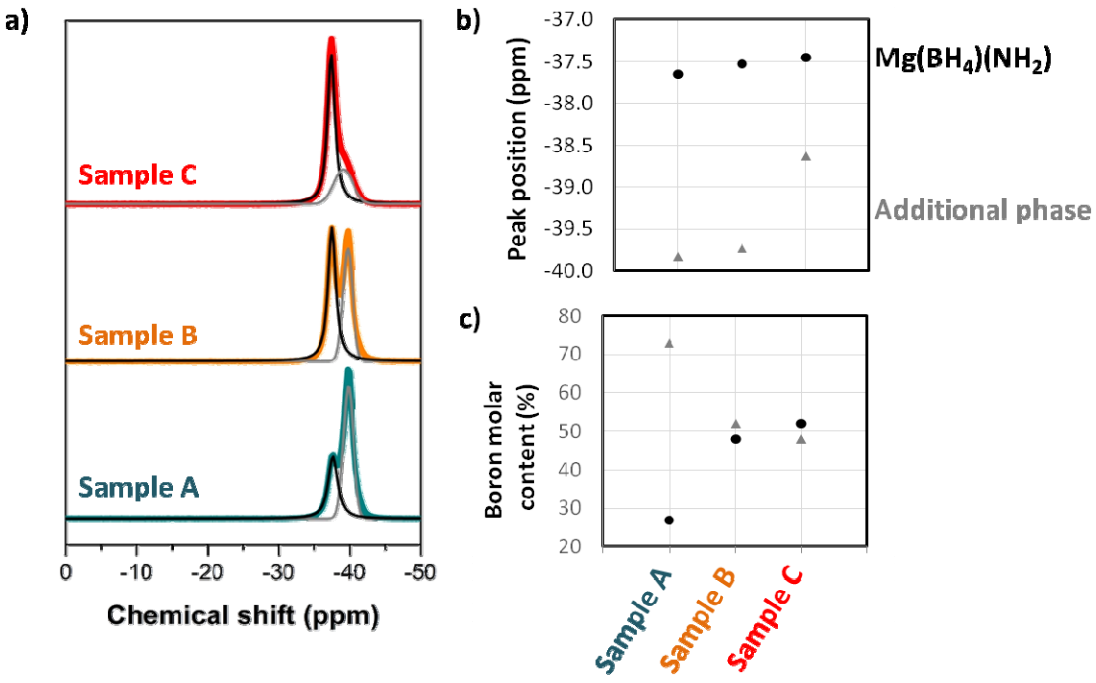

Figure 2. (a) ^{11}B MAS-NMR spectra for the samples A, B and C. **(b)** Peaks position in ppm attributed to $Mg(BH_4)(NH_2)$ and the additional phase. **(c)** Molar percentages of boron contributing to each peak. The 95% confidence interval of the fit is contained in the symbols.

If we consider that this additional phase has a different stoichiometry such as $Mg_{x+y}(BH_4)_{2x}(NH_2)_{2y}$, the difference in the number of $(NH_2)^-$ groups surrounding $(BH_4)^-$ would have a shielding or deshielding effect of the boron atoms. This effect has already been observed by Yang et al. for the $Mg(BH_4)_2.xNH_3$ phases.[28] When x increases in these phases, the chemical shift observed for the $(BH_4)^-$ group is gradually reduced to lower values from -39.6 ppm for x = 0 to -37.1 ppm for x = 6, i.e. a deshielding effect on the boron atoms. In our present study, the boron atoms in the additional phase (-39.6 ppm) are more shielded than the boron atoms in $Mg(BH_4)(NH_2)$ and, more similar to the boron atoms encountered in $Mg(BH_4)_2$ (-39.5 ppm for γ-$Mg(BH_4)_2$, cf. Figure S3). Under the assumption that the contribution of the $(NH_2)^-$ groups to the ^{11}B chemical shift is similar, we can predict that the composition of the additional phase should be $Mg_{x+y}(BH_4)_{2x}(NH_2)_{2y}$ with x > y.

In the case of sample C, for which only $Mg(BH_4)(NH_2)$ was observed by XRD (cf. Figure 1), only one peak was expected on the NMR spectrum as, in the crystal structure

reported for $Mg(BH_4)(NH_2)$, the boron atoms occupy a single Wyckoff site. Two NMR peaks are however detected: the first peak (52 molar % of the boron in the sample) at -37.6 ppm is similar to samples A and B and confirms the assignment. The second peak (48 molar %) differs from that in the other samples: it is slightly less shielded at -38.6 ppm (cf. Figure 2b) and the quadrupolar coupling parameters are very different (cf. Table S2). The slight deshielding compared to the additional phase in samples A and B suggests, under the same assumption as before, a composition slightly richer in NH_2 ($Mg_{x+z}(BH_4)_{2z}(NH_2)_{2z}$ with x >z> y).

Additional information as crystallinity degree can be extracted from the Full Width at Half Maximum (FWHM) of the NMR peaks. The FWHM is in between 1.2-1.7 ppm for all peaks except for the additional phase in sample C which has a value of 3.8 ppm. This peak broadening and the pure Gaussian shape reveal the amorphous character of the new additional phase in sample C, this sample being considered as pure $Mg(BH_4)(NH_2)$ from XRD analyses. The very amorphous character of this additional phase explains the difficulty for its observation by XRD; even if it represents 48 molar % of the total boron atoms. Further NMR experiments, including ^{15}N MAS, are in progress to look further at the environment of the $(BH_4)^-$ groups and to elucidate the exact nature of the additional phases.

Hence, from sample A to sample C, the $Mg(BH_4)(NH_2)$ content increases and the part of an additional phase, whom stoichiometry can be predicted as $Mg_{x+y}(BH_4)_{2x}(NH_2)_{2y}$ with x > y, decreases. In sample C, the additional phase is probably slightly richer in NH_2. These quantities and structural variations could affect the conduction properties as described in the next parts.

3.3. Ionic conductivity

The ionic conductivities were measured by Electrochemical Impedance Spectroscopy on pellets made from powders of the samples A, B and C. Measurements were not performed at temperatures higher than 100°C to avoid thermal degradation. Indeed, our samples show endothermic phenomena between 120°C and 170°C (cf. Figure S4). These phenomena can be related to an amorphization as described by Noritake et al.[15] Figure 3a exhibits the Nyquist and the Bode plots at 100°C. For each sample, a semi-circle can be observed on the Nyquist plot at high frequencies with the presence of a semi-circle weakly marked at middle frequencies. At lower frequency, a more vertical straight line (capacitive effect) characteristic

of ion-blocking electrodes (Papyex foils) can be observed. This line is not perfectly vertical due to the surface roughness.

XRD and ^{11}B MAS-NMR analyses showed that each sample contains $Mg(BH_4)(NH_2)$ and an additional phase. By a simple observation of the Nyquist diagrams, it can be noticed that the proportion of the second phenomenon at middle frequencies increases with the quantity of the additional phase. The observation at high and middle frequencies clearly shows the presence of two phenomena as also very well seen on the phase Bode plots (cf. Figure 3a): these plots enable us to separate the two phenomena in frequency range. The second phenomenon is very minor in the case of sample C with a low peak intensity at around 10 Hz. So we could consider that the two observed conduction phenomena are due to the ionic conduction in the two phases. With an appropriate equivalent circuit, we can extract the conductivity, activation energy and the real capacitance as a function of temperature to attribute the physical meaning of each phenomenon and correlate them with the results obtained by the other characterization techniques described previously.

The sample preparation by ball-milling involves a good mixing of the different precursors. As the thermal treatment is performed on pellets, and the different phases are generated during this thermal treatment, we could consider that $Mg(BH_4)(NH_2)$ is the grain and the additional phase the grain boundaries as in a brick layer model. By taking this model into account, the fitting of impedance signals were performed with the equivalent circuit shown on Figure 3b. The equivalent circuit is composed of an initial resistor R_0 for the device and current collectors resistance, in series with a first $R_1//CPE_1$ (R_1 for the bulk solid electrolyte resistance in parallel with a constant phase element CPE_1 for the non-ideal capacitance) and a second $R_2//CPE_2$ for the grain boundaries conduction (resistance and capacitance) and, finally, another constant phase element (CPE_3) for the impedance of both the top and bottom electrode-electrolyte junctions to consider the roughness of the electrical contact. To obtain a good fit, it was not necessary to consider an interface between the Papyex foils and the solid electrolyte. As described previously, R_1 could be associated to the conduction of $Mg(BH_4)(NH_2)$ and R_2 to the grain boundaries constituted by the additional phase. This hypothesis will be verified thereafter by the evolution of the real capacitance as a function of temperature.

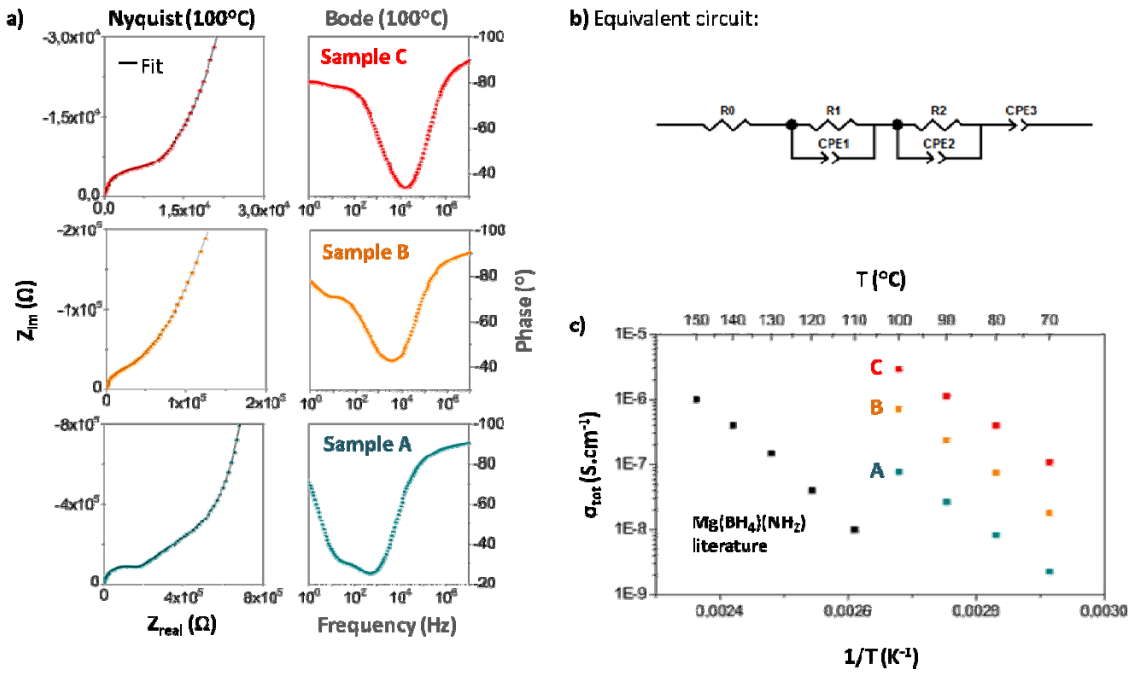

Figure 3. EIS measurements for the samples A, B and C. **(a)** Nyquist plots and Bode plots at 100°C, **(b)** Equivalent circuit used to model the results, **(c)** Arrhenius plots of the total ionic conductivity compared to the values reported for $Mg(BH_4)(NH_2)$ (black dots).[12]

Once R_1 and R_2 are determined by fitting the model with the experimental data and knowing the thickness (l) and the surface (S) of our pellets, the total ionic conductivity (σ_{tot}) can be calculated from the equation 1:

$$\sigma = \frac{1}{(R_1 + R_2)} * \frac{l}{S} \qquad \text{(eq. 1)}$$

A reduction of the total resistance is noticed upon heating revealing the enhancement of the ionic conductivity with temperature. For the three samples, the ionic conductivities follow a linear Arrhenius behavior when log(σ) is plotted as function of 1/T as represented in Figure 3c. The total ionic conductivity increases as the sample purity is improved (i.e. higher $Mg(BH_4)(NH_2)$ content).

Very interestingly, the ionic conductivity reaches $3x10^{-6}$ $S.cm^{-1}$ at 100°C for sample C. This conductivity is more than three orders of magnitude higher than the one reported by Higashi et al.[12] for the same compound (cf. black dots on Figure 3c). This value of ionic conductivity is one of the highest reported at this temperature, getting close to the one

obtained by Roedern et al. for $Mg(en)_1(BH_4)_2$ with *en* being ethylene-diamine molecule.[11] These results could be explained by the presence of the additional phase. Especially, once this phase gets amorphous as shown by ^{11}B MAS-NMR spectroscopy, it would create a glass-ceramic-like composite material with improved ionic conduction, as previously described by Tsukasaki et al. on $Li_2S–P_2S_5$ glass-ceramics.[29] In their study, nano-crystals of Li_3PS_4 were observed by TEM within an amorphous matrix in $Li_2S–P_2S_5$ glass-ceramics explaining the improvement in ionic conductivity compared to the glasses. This assumption is also supported in our study by the fact that the ionic conductivity of the pellet decreases with the increase of the proportion of crystalline additional phase. The enhancement of the ionic conductivity can also be related to the study of Yan et al. in which they demonstrate that adding an excess of BH_4 in $Li_4(BH_4)(NH_2)_3$ would create a solid solution with disorder in the structure which enables fast Li^+ diffusion[30]. In our case, the $Mg(BH_4)(NH_2)$-based composite material could have a similar behavior.

The conduction phenomena at high and middle frequencies can be separated by the equivalent circuit described previously. To extract the activation energy (Ea) of each phenomenon, $\ln(\sigma.T)$ is plotted as a function of 1/T for each sample as shown on Figure 4a. A clear difference of behavior can be observed for the two phenomena. Ea for the middle frequency phenomenon remains constant around 1.3 eV whereas the one at high frequency decreases as the sample is getting higher purity in $Mg(BH_4)(NH_2)$, evolving from 1.3 eV to 1.0 eV, which confirms our attribution of $Mg(BH_4)(NH_2)$ as the grain in our model. These Ea values are similar to those reported in the literature for the same material (1.31 eV) and other Mg^{2+} ion conductors.[8,11]

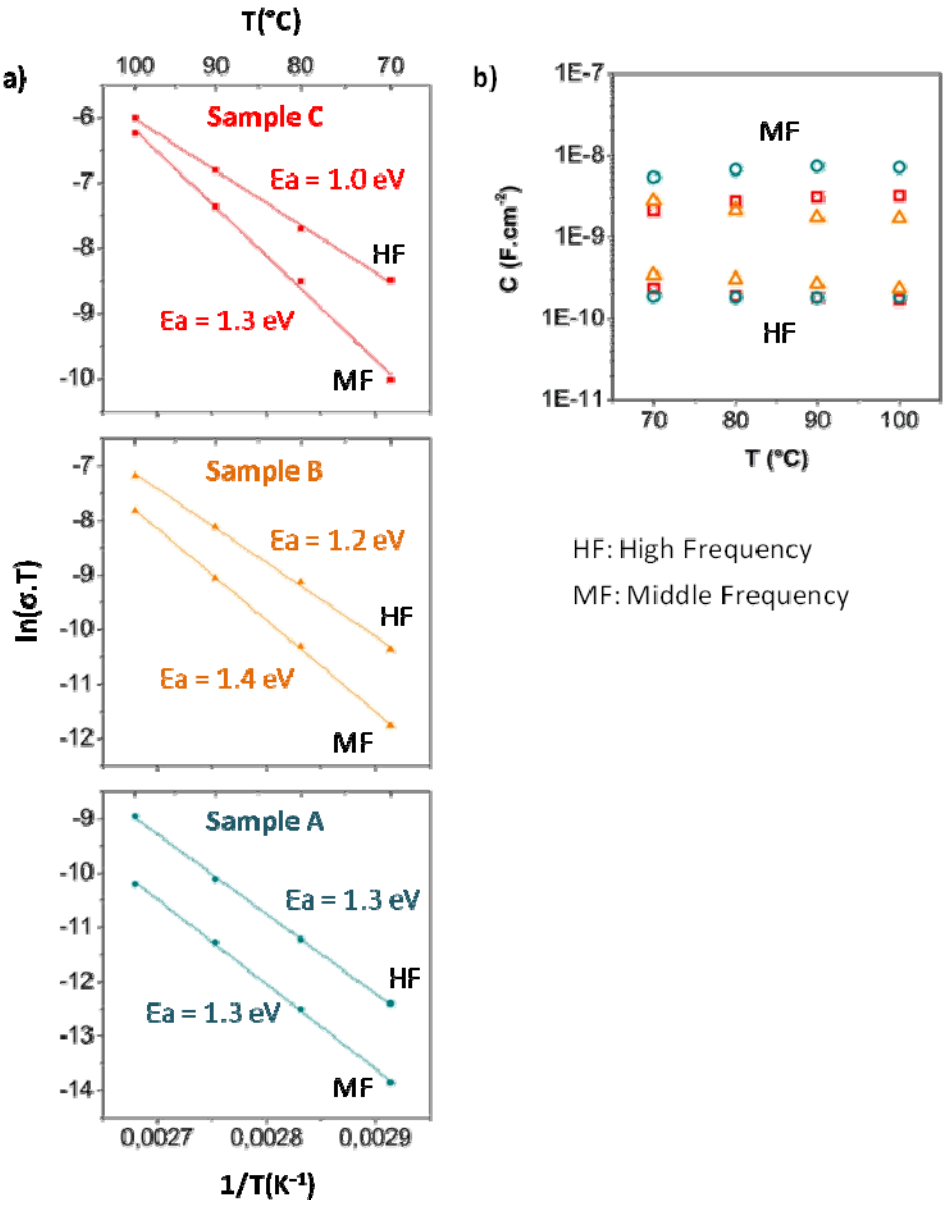

Figure 4. (a) ln(σ.T) = f(1/T) used to calculate the activation energies of the two ionic conduction phenomena (at high and middle frequency), **(b)** Capacitance values for the two conduction phenomena as a function of the temperature.

To evaluate our fit, model and physical meaning, the real capacitance values of each conduction phenomenon is extracted for the R//CPE couple. The complex impedance of a CPE is expressed by the following equation:

$$Z_{CPE} = \frac{1}{Y_0 (j\omega)^n} \qquad \text{(eq. 2)}$$

and:

$$R = \frac{1}{Y_0 * \omega^n} \quad \text{and} \quad R = \frac{1}{C * \omega} \qquad \text{(eq. 3 and 4)}$$

So with equations (2), (3) and (4), it can be written:

$$C = R^{\frac{1-n}{n}} * Y_0^{\frac{1}{n}} \qquad \text{(eq. 5)}$$

where R and C are respectively the resistance and the real capacitance related to the conduction phenomenon, Y_0 is the prefactor of the CPE and n is a factor (included to define CPE element) comprised between 1 and 0, this value depending on several parameters such as the surface roughness or a non-uniform current distribution. The real calculated capacitances for each phenomenon are plotted versus the temperature on Figure 4b. For the phenomenon at middle frequency, a real capacitance of $3x10^{-9}$ F.cm^{-2} is obtained whereas for the one at high frequency the real capacitance is around $1.8x10^{-10}$ F.cm^{-2}. These capacitance values are typical of ionic conduction phenomena and, hence, confirm our assumption that the high and middle frequencies phenomena are due to the ionic conduction in both phases and not to the formation of interfaces. For each sample and phenomenon, the real capacitance remains constant as a function of temperature, which is scientifically sound as the capacitance is only dependent on the electrical permittivity of the phase and its geometrical dimensions, these parameters being independent of the temperature. It can be noticed, that the real capacitance of the phenomenon at higher frequency is the same for the three samples, whose common feature is the presence of the $Mg(BH_4)(NH_2)$ phase. The real capacitance value for the phenomenon at middle frequencies changes slowly as a function of the crystallinity of the additional phase. Hence, these results validate our equivalent circuit and assumption as the conduction properties of $Mg(BH_4)(NH_2)$ can be extracted from higher frequencies and conduction properties of the additional phase considered as grain boundaries at middle frequencies. The crystallinity of this additional phase modifies considerably the conduction properties of the material. The higher ionic conductivity is obtained with a glass-ceramic like composite material with crystalline $Mg(BH_4)(NH_2)$ embedded into the amorphous additional phase.

4. CONCLUSIONS

$Mg(BH_4)(NH_2)$ was prepared from $Mg(BH_4)_2$ and $Mg(NH_2)_2$ by ball-milling and further annealing. The synthesis parameters were carefully investigated. An additional phase was formed at low ball-milling speed whereas $Mg(BH_4)(NH_2)$ supposedly pure from X-ray diffraction was obtained when increasing the milling speed. Meanwhile, ^{11}B MAS-NMR spectroscopy revealed that the additional phase, also containing the $(BH_4)^-$ anion, is still present under an amorphous form for the sample obtained at high ball milling speed.

The ionic conductivity determined by Electrochemical Impedance Spectroscopy for the purest $Mg(BH_4)(NH_2)$ sample was found to be $3x10^{-6}$ S.cm^{-1} at 100°C which is more than three orders of magnitude higher than that previously reported.[12] This improvement could be due to the presence of the amorphous additional phase creating a glass-ceramic-like composite material. This assumption is supported by the fact that when the additional phase is crystalline, the ionic conductivity of the sample is lower. The activation energy of the ionic conductivity is of the order of 1.2-1.3 eV.

Further work is needed to understand what is the exact nature of the additional phase which could be a new compound of composition $Mg_{x+y}(BH_4)_{2x}(NH_2)_{2y}$. The observed enhancement in the ionic conductivity of $Mg(BH_4)(NH_2)$ is encouraging and works are under way for using this material as a solid-state electrolyte of rechargeable Mg batteries.

Acknowledgments

The RS2E (French network on electrochemical energy storage) is acknowledged for the PhD funding of Ronan Le Ruyet (STORE-EX Labex Project ANR-10-LABX-76-01). Financial support from the TGIR-RMN-THC FR 3050 CNRS for conducting the solid-state MAS-NMR spectroscopy is gratefully acknowledged.. The authors thank M. Yon (CEMHTI) for providing the home-made MATLAB program for NMR baseline correction. Matthieu Courty (LRCS, Amiens) is thanked for the thermal analysis done by DSC calorimetry and gas mass spectroscopy.

Supporting information

- Table of synthesis parameters tried to obtain $Mg(BH_4)(NH_2)$.
- PXRD pattern of the samples obtained after different ball-milling and annealing conditions.
- ^{11}B MAS-NMR spinning sideband patterns for the samples A, B and C, the model and the fit parameters of the model.
- ^{11}B MAS-NMR spectrum of γ-$Mg(BH_4)_2$.
- DSC measurements of sample A, B and C.
- Gas mass spectrometry of sample C.

References

(1) Yoo, H. D.; Shterenberg, I.; Gofer, Y.; Gershinsky, G.; Pour, N.; Aurbach, D. Mg Rechargeable Batteries: An on-Going Challenge. *Energy Environ. Sci.* **2013**, *6* (8), 2265-2279.

(2) Aurbach, D.; Lu, Z.; Schechter, A.; Gofer, Y.; Gizbar, H.; Turgeman, R.; Cohen, Y.; Moshkovich, M.; Levi, E. Prototype Systems for Rechargeable Magnesium Batteries. *Nature* **2000**, *407* (6805), 724-727.

(3) Muldoon, J.; Bucur, C. B.; Oliver, A. G.; Sugimoto, T.; Matsui, M.; Kim, H. S.; Allred, G. D.; Zajicek, J.; Kotani, Y. Electrolyte Roadblocks to a Magnesium Rechargeable Battery. *Energy Environ. Sci.* **2012**, *5* (3), 5941-5950.

(4) Mohtadi, R.; Mizuno, F. Magnesium Batteries: Current State of the Art, Issues and Future Perspectives. *Beilstein J. Nanotechnol.* **2014**, *5* (1), 1291-1311.

(5) Mohtadi, R.; Matsui, M.; Arthur, T. S.; Hwang, S.-J. Magnesium Borohydride: From Hydrogen Storage to Magnesium Battery. *Angew. Chemie Int. Ed.* **2012**, *51* (39), 9780-9783.

(6) Tutusaus, O.; Mohtadi, R.; Arthur, T. S.; Mizuno, F.; Nelson, E. G.; Sevryugina, Y. V. An Efficient Halogen-Free Electrolyte for Use in Rechargeable Magnesium Batteries. *Angew. Chemie Int. Ed.* **2015**, *54* (27), 7900-7904.

(7) Yamanaka, T.; Hayashi, A.; Yamauchi, A.; Tatsumisago, M. Preparation of Magnesium Ion Conducting MgS-P_2S_5-MgI_2 Glasses by a Mechanochemical Technique. *Solid State Ionics* **2013**, *262*, 601-603.

(8) Ikeda, S.; Takahashi, M.; Ishikawa, J.; Ito, K. Solid Electrolytes with Multivalent Cation Conduction. 1. Conducting Species in Mg-Zr-PO_4 System. *Solid State Ionics* **1987**, *23* (1-2), 125-129.

(9) Kawamura, J.; Morota, K.; Kuwata, N.; Nakamura, Y.; Maekawa, H.; Hattori, T.; Imanaka, N.; Okazaki, Y.; Adachi, G. High Temperature ^{31}P NMR Study on Mg^{2+} Ion Conductors. *Solid State Commun.* **2001**, *120* (7-8), 295-298.

(10) Imanaka, N.; Okazaki, Y.; Adachi, G. Divalent Magnesium Ion Conducting Characteristics in Phosphate Based Solid Electrolyte Composites. *J. Mater. Chem.* **2000**, *10* (6), 1431-1435.

(11) Roedern, E.; Kühnel, R.-S.; Remhof, A.; Battaglia, C. Magnesium Ethylenediamine Borohydride as Solid-State Electrolyte for Magnesium Batteries. *Sci. Rep.* **2017**, *7* (1), 46189.

(12) Higashi, S.; Miwa, K.; Aoki, M.; Takechi, K. A Novel Inorganic Solid State Ion Conductor for Rechargeable Mg Batteries. *Chem. Commun.* **2014**, *50* (11), 1320-1322.

(13) Matsuo, M.; Remhof, A.; Martelli, P.; Caputo, R.; Ernst, M.; Miura, Y.; Sato, T.; Oguchi, H.; Maekawa, H.; Takamura, H.; et al. Complex Hydrides with $(BH_4)^-$ and $(NH_2)^-$ Anions as New Lithium Fast-Ion Conductors. *J. Am. Chem. Soc.* **2009**, *131* (45), 16389-16391.

(14) Noritake, T.; Miwa, K.; Aoki, M.; Matsumoto, M.; Towata, S.; Li, H.-W.; Orimo, S. Synthesis and Crystal Structure Analysis of Complex Hydride $Mg(BH_4)(NH_2)$. *Int. J. Hydrogen Energy* **2013**, *38* (16), 6730-6735.

(15) Noritake, T.; Miwa, K.; Aoki, M.; Matsumoto, M.; Towata, S.; Li, H.-W.; Orimo, S. Dehydrogenation Properties and Crystal Structure Analysis of $Mg(BH_4)(NH_2)$. *J. Alloys Compd.* **2013**, *580* (15), S85-S89.

(16) Yang, Y.; Liu, Y.; Zhang, Y.; Li, Y.; Gao, M.; Pan, H. Hydrogen Storage Properties and Mechanisms of $Mg(BH_4)_2.2NH_3$–$xMgH_2$ Combination Systems. *J. Alloys Compd.* **2014**, *585* (22), 674-680.

(17) Leng, H. Y.; Ichikawa, T.; Hino, S.; Hanada, N.; Isobe, S.; Fujii, H. Synthesis and Decomposition Reactions of Metal Amides in Metal–N–H Hydrogen Storage System. *J. Power Sources* **2006**, *156* (2), 166-170.

(18) Ma, L.; Dai, H.; Fang, Z.; Kang, X.; Liang, Y.; Wang, P.-J.; Wang, P.; Cheng, H. Enhanced Hydrogen Storage Properties of Li-Mg-N-H System Prepared by Reacting $Mg(NH_2)_2$ with Li_3N. *J. Phys. Chem. C* **2009**, *113* (22), 9944-9949.

(19) Nakamori, Y.; Kitahara, G.; Orimo, S. Synthesis and Dehydriding Studies of Mg-N-H

Systems. *J. Power Sources* **2004**, *138* (1-2), 309-312.

(20) Leriche, J. B.; Hamelet, S.; Shu, J.; Morcrette, M.; Masquelier, C.; Ouvrard, G.; Zerrouki, M.; Soudan, P.; Belin, S.; Elkaïm, E.; et al. An Electrochemical Cell for Operando Study of Lithium Batteries Using Synchrotron Radiation. *J. Electrochem. Soc.* **2010**, *157* (5), A606-A610.

(21) Massiot, D.; Fayon, F.; Capron, M.; King, I.; Le Calvé, S.; Alonso, B.; Durand, J.; Bujoli, B.; Gan, Z.; Hoatson, G. Modelling One- and Two-Dimensional Solid-State NMR Spectra. *Magn. Reson. Chem.* **2002**, *40* (1), 70-76.

(22) Zhou, Y.; Matsuo, M.; Miura, Y.; Takamura, H.; Maekawa, H.; Remhof, A.; Borgschulte, A.; Züttel, A.; Otomo, T.; Orimo, S. Enhanced Electrical Conductivities of Complex Hydrides $Li_2(BH_4)(NH_2)$ and $Li_4(BH_4)(NH_2)_3$ by Melting. *Mater. Trans.* **2011**, *52* (4), 654-657.

(23) Borgschulte, A.; Jones, M. O.; Callini, E.; Probst, B.; Kato, S.; Züttel, A.; David, W. I. F.; Orimo, S. Surface and Bulk Reactions in Borohydrides and Amides. *Energy Environ. Sci.* **2012**, *5* (5), 6823-6832.

(24) Remhof, A.; Yan, Y.; Rentsch, D.; Borgschulte, A.; Jensen, C. M.; Züttel, A. Solvent-Free Synthesis and Stability of $MgB_{12}H_{12}$. *J. Mater. Chem. A* **2014**, *2* (20), 7244-7249.

(25) Huang, J.; Yan, Y.; Remhof, A.; Zhang, Y.; Rentsch, D.; Au, Y. S.; de Jongh, P. E.; Cuevas, F.; Ouyang, L.; Zhu, M.; et al. A Novel Method for the Synthesis of Solvent-Free $Mg(B_3H_8)_2$. *Dalt. Trans.* **2016**, *45* (9), 3687-3690.

(26) Au, Y. S.; Yan, Y.; de Jong, K. P.; Remhof, A.; de Jongh, P. E. Pore Confined Synthesis of Magnesium Boron Hydride Nanoparticles. *J. Phys. Chem. C* **2014**, *118* (36), 20832-20839.

(27) David, W. I. F.; Callear, S. K.; Jones, M. O.; Aeberhard, P. C.; Culligan, S. D.; Pohl, A. H.; Johnson, S. R.; Ryan, K. R.; Parker, J. E.; Edwards, P. P.; et al. The Structure, Thermal Properties and Phase Transformations of the Cubic Polymorph of Magnesium Tetrahydroborate. *Phys. Chem. Chem. Phys.* **2012**, *14* (33), 11800-11807.

(28) Yang, Y.; Liu, Y.; Li, Y.; Gao, M.; Pan, H. Synthesis and Thermal Decomposition Behaviors of Magnesium Borohydride Ammoniates with Controllable Composition as Hydrogen Storage Materials. *Chem. Asian J.* **2013**, *8* (2), 476-481.

(29) Tsukasaki, H.; Mori, S.; Morimoto, H.; Hayashi, A.; Tatsumisago, M. Direct Observation of a Non-Crystalline State of Li_2S–P_2S_5 Solid Electrolytes. *Sci. Rep.* **2017**, *7*, 4142.

(30) Yan, Y.; Kühnel, R.; Remhof, A.; Duchêne, L.; Reyes, E. C.; Rentsch, D.; Łodziana,

Z.; Battaglia, C. A Lithium Amide-Borohydride Solid-State Electrolyte with Lithium-Ion Conductivities Comparable to Liquid Electrolytes. *Adv. Energy Mater.* **2017**, *1700294*, 1-7.

TOC Graphic

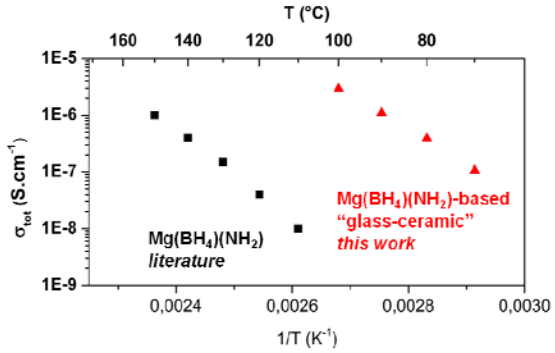
T (°C)
160
140
120
100
80
1E-5
1E-6
1E-7
1E-8
1E-9
σtot (S.cm-1)
Mg(BH4)(NH2)
literature
Mg(BH4)(NH2)-based
"glass-ceramic"
this work
0,0024
0,0026
0,0028
0,0030
1/T (K-1)